Insights and Lessons Learned from the NASA Juncture Flow Experiment

Christopher L. Rumsey
NASA Langley Research Center
Hampton, VA 23681
USA

c.l.rumsey@nasa.gov

ABSTRACT

The NASA Juncture Flow experiment involved both CFD and wind tunnel measurements in its quest to provide CFD validation data for separated flow in a wing-fuselage corner. The experience has produced not only a wealth of valuable validation data and a new version of a turbulence model, it also yielded many lessons learned. This paper conveys those insights, particularly with respect to the qualities we believe to be essential in a CFD validation experiment. These include wind tunnel characterization and use of CFD as an assessment tool during the validation process. With a considerable number of validation tests already run both by the NASA team as well as by independent groups, a brief assessment is made of CFD's current ability to predict the corner flow separation.

1.0 INTRODUCTION

The NASA Juncture Flow (JF) CFD validation experiment represents a concerted effort to obtain measured wind tunnel data for a separated corner in subsonic flow conditions. The separation occurs near the trailing edge junction of a wing and fuselage; its extent is a function of the test article's angle of incidence. This type of flow separation is of interest to the aerospace community because it can occur on many vehicles where two surfaces intersect to form a junction. Furthermore, most of today's state-of-the-art CFD methods typically do not predict the onset and progression of this type of junction separation correctly or consistently [1,2], so reliable flowfield data are needed to help guide future improvements to the CFD models. The experiment is specifically geared toward supporting CFD validation efforts.

Validation is clearly defined as *"the process of determining the degree to which a model is an accurate representation of the real world from the perspective of the intended uses of the model"* [3]. However, it is not as clear what is precisely meant by a CFD validation experiment, so we make reference to a few different definitions. The first is from Lee et al. [4], which states:

"A validation experiment is a physical realization of a properly posed applied mathematics problem with initial conditions, boundary conditions, material properties, and external forces" and "Validation experiments are performed to generate data for assessing the accuracy of the mathematical model via simulation outcomes produced by the verified computational model."

In Oberkampf and Smith [5], they say:

"A validation experiment is conducted for the primary goal of determining the predictive capability of a mathematical model of a physical process."

A somewhat different perspective is given by Taylor and Rumsey [6]:

"A CFD validation experiment is the process followed from the point at which physical phenomena of interest are first identified, through to that at which the results of CFD computations are compared with physical measurements in a manner that is designed specifically to assess CFD predictive capability."

Combining these definitions, we make the assertion that the validation experiment consists of both physical testing and CFD efforts working in tandem toward the common goal of assessing (and hopefully improving) CFD predictive capability. From Ref. [6], the process involves two key enablers: validation dialog and technique verification. The validation dialog consists of a close, synergistic relationship between the computational and physical testing activities throughout the experimental effort. Technique verification includes code and solution verification on the CFD side, and the establishment of reference conditions and measurement parameters on the physical testing side, including uncertainty quantification. Some details can be found in the abovementioned paper.

In the NASA JF effort, the physical testing was conducted on a full-span, sting-mounted wing-body configuration (with truncated F6 wing shape and flat-sided fuselage) in the NASA Langley Research Center 14- by 22-Foot Subsonic Tunnel (14x22). Characterization of the wind tunnel test – measuring all of the important characteristics that are needed for input to the computational simulation – is one of the most important aspects of the physical testing. Otherwise, one is never sure whether differences between CFD and physical measurements are caused solely by the turbulence model, or whether a mischaracterized boundary condition or incorrect geometric shape is also a contributing factor. In the JF experiment, attempts were made to document many of the wind tunnel characteristics, including wind tunnel shape and boundary conditions, model deflections, as-built model shape, and tripping/transition behavior. The validation data itself was achieved primarily via laser doppler velocimetry (LDV), particle image velocimetry (PIV), oil flow, and surface pressure measurements [7-9].

A photograph of the NASA JF model is shown in Figure 1, and sketches of the model in the 14x22 wind tunnel are provided in Figures 2, 3, and 4. The first wind tunnel entry of the NASA JF model was completed in 2018, and results were documented in Kegerise and Neuhart [7] as well as on the NASA Langley Turbulence Modeling Resource (TMR) website [8]. A second wind tunnel entry was completed in early 2020. Its results were documented in Rumsey et al. [9] as well as on the TMR website. There have also been many CFD efforts focused on this configuration [10-13], including some that appeared in an AIAA special session at SciTech in 2020 [14-20], some in a special session at AIAA Aviation in 2020 [21-25], and some at AIAA SciTech 2021 [26-29]. As a result of the wind tunnel tests and CFD efforts to date, we have gained a significant amount of insight into this flow, and have also established some lessons learned regarding both the physical testing and the CFD. The purpose of this paper is to highlight these insights and lessons learned. Many of them relate to the use of a wind tunnel in the data collection process, along with issues regarding the importance of assessing the impact of wind tunnel modeling in the CFD.

2.0 WIND TUNNEL CHARACTERIZATION

Quantifying the incoming boundary conditions in a major wind tunnel facility like the 14x22 is very challenging because of lack of optical access and the large area involved. As part of the NASA JF project, the Boeing Quantitative Wake Survey System (QWSS) [30] was used in an attempt to measure the incoming flow characteristics near the start of the 15.24 m test section, in spite of the fact that this was outside of the QWSS's intended use [12]. The tests confirmed the presence of a known total pressure deficit near the center region of the

tunnel, which has also been noted in other major wind tunnels [31]. The reason for the deficit is not known. The magnitude of this deficit varies with tunnel dynamic pressure. Results in terms of $\Delta p_t = p_{t,probe} - p_{t,ref}$ in Figure 5 indicate that there is approximately a 1 psf total pressure deficit at the JF conditions. To date, a method for specifying a variable total pressure boundary condition using a momentum sink disk has been attempted by the JF team in unpublished CFD studies for the purpose of comparing with QWSS measurements in the test section. However, the method has not yet been used to perform parametric studies to determine the influence of the total pressure variation on the JF quantities of interest. Because the junction region of focus is very localized near the tunnel centerline, the impact for JF is likely to be very small.

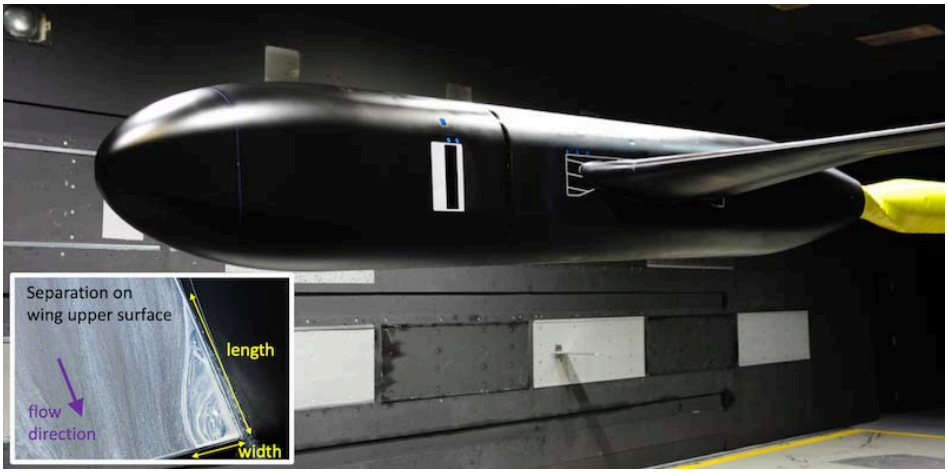

Figure 1. The NASA JF model, with inset photograph of oil flow showing separation on the upper surface wing junction at 5° angle of incidence.

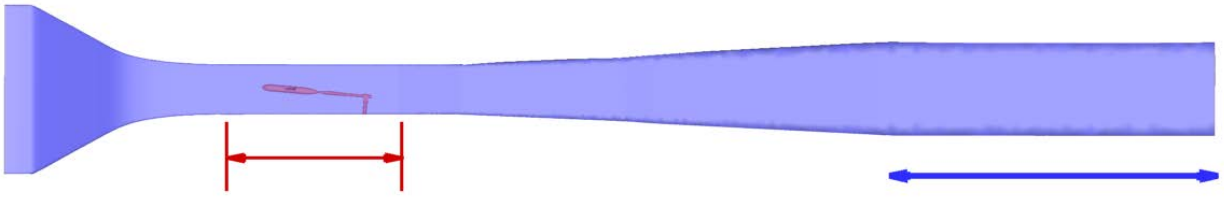

Figure 2. Sketch of the NASA JF model in the 14x22 tunnel; red arrow represents start and end of test section; blue arrow indicates "CFD extension" used in computations to avoid separation at the outflow boundary.

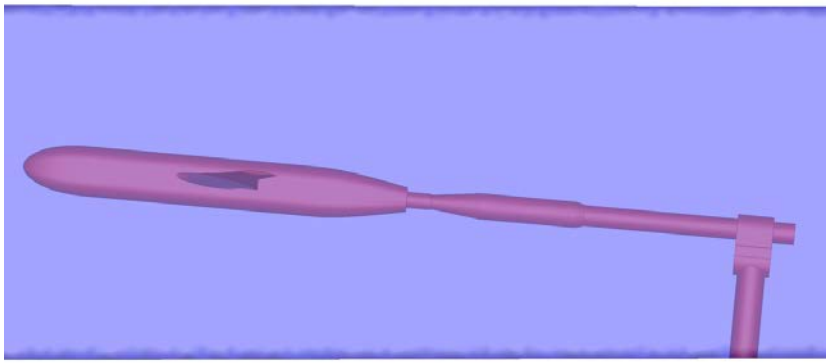

Figure 3: Sketch of NASA JF model in the 14x22 tunnel at 5 degrees angle of incidence, side view.

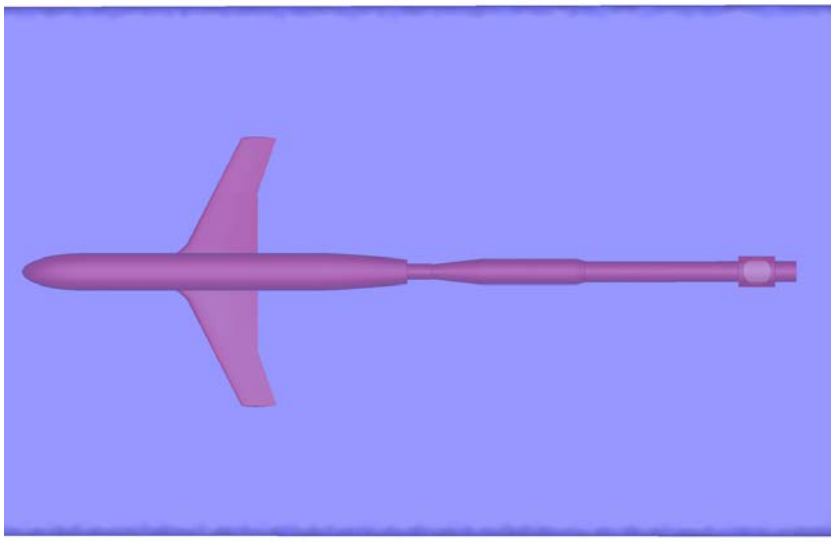

Figure 4: Sketch of NASA JF model in the 14x22 tunnel, top view.

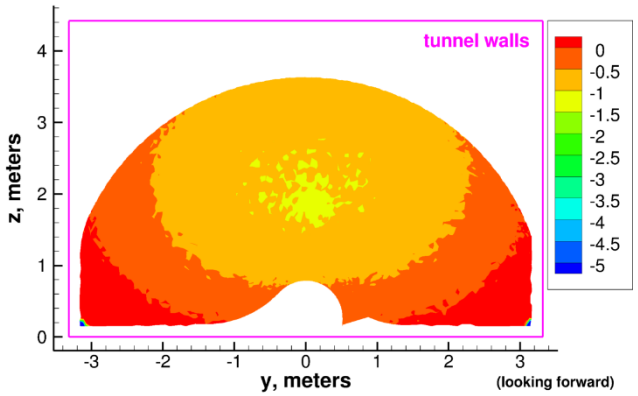

Figure 5: Tunnel total pressure deficit (psf) measured by QWSS at Q=60 psf, 1.615 m downstream of the start of the empty 14x22 test section.

There were no clear trends from the QWSS data showing major consistent flow angularity deviations in the 14x22; angularity deviations from expected flow over most of the tunnel cross section were well less than 1 degree [12]. But the accuracy of the QWSS freestream angularity measurement is unclear, and is still under investigation. Also, it is important to note that the QWSS could not access a large area of the 14x22 tunnel cross section, as seen by the white regions in Figure 5. For reference, note that the tunnel wall boundary layer thickness has been measured to be approximately 100-125 mm thick near the *x*-location shown in Figure 5. Thus, the QWSS measurements were well outside of the tunnel's boundary layers, although some evidence of corner vortices appears to be visible in the plot near the bottom left and right corners.

Despite the difficulties associated with measuring tunnel inflow details, measurements of tunnel wall boundary-layer thickness at several locations have proved to be useful for CFD validation checks when modeling the tunnel walls. For example, including the upstream tunnel contraction in the CFD (starting near the screens), as shown in Figure 2, was found to yield computed tunnel wall boundary-layer thicknesses consistent with the experiment.

Measurements of wall pressures in the wind tunnel diffuser have not been as useful for CFD, because CFD sets its own back pressure in order to obtain flow conditions in the test section that are consistent with the experiment. However, comparisons in an empty tunnel between CFD and wind tunnel measurements in the diffuser were consistent [12]. As a complication, we have found that spurious separation can sometimes occur in the CFD diffuser that may not necessarily correspond with the flow in the wind tunnel's diffuser [12]. However, as long as the flow in the test section is consistent, then spurious separations far downstream in the diffuser appear to have no noticeable impact on the quantities of interest on the test article. Strategies for running CFD tunnel cases in the presence of possible spurious separation will be discussed in the next section.

Measurements of tunnel side and top wall pressures have been included in the JF wind tunnel characterization dataset. Like the diffuser pressures, these have had limited usefulness for CFD to date, as they do not provide information that is directly needed in any CFD boundary condition. However, they can provide a check on the character and quality of the CFD wind tunnel simulations. The wall pressures are provided in terms of pressure coefficient, c_p, for which the reference conditions are obtained via tunnel calibration equations. In Figure 6, CFD tunnel wall pressure coefficients are compared with wind tunnel (WT) measurements with the JF test article present. These WT results represent an approximate fit to measured data from many tunnel runs. The CFD trends

in c_p are consistent with the measurements, but they are consistently high, near the upper uncertainty bounds of the measured values. It is possible that this consistent shift is due to the fact that the CFD simulation does not currently account for the tunnel's total pressure deficit described earlier. This issue is still under investigation. It should also be noted that the 14x22 wall static pressure orifices are not pristine orifices, and were always intended to be used with a tare process and not for direct comparison purposes.

The shape of the 14x22 high-speed leg was extracted from laser scan data [32]. In the process, it was also simplified to some degree: notches, grooves, windows, and other relatively small deviations in the tunnel walls were smoothed over, with the assumption that they have very little impact on the global flowfield. In Ref. [32], it was shown that use of this "as-built" geometry in CFD empty tunnel simulations was far superior to the use of the "as-designed" geometry (from construction drawings) for predicting upwash angles in the test section.

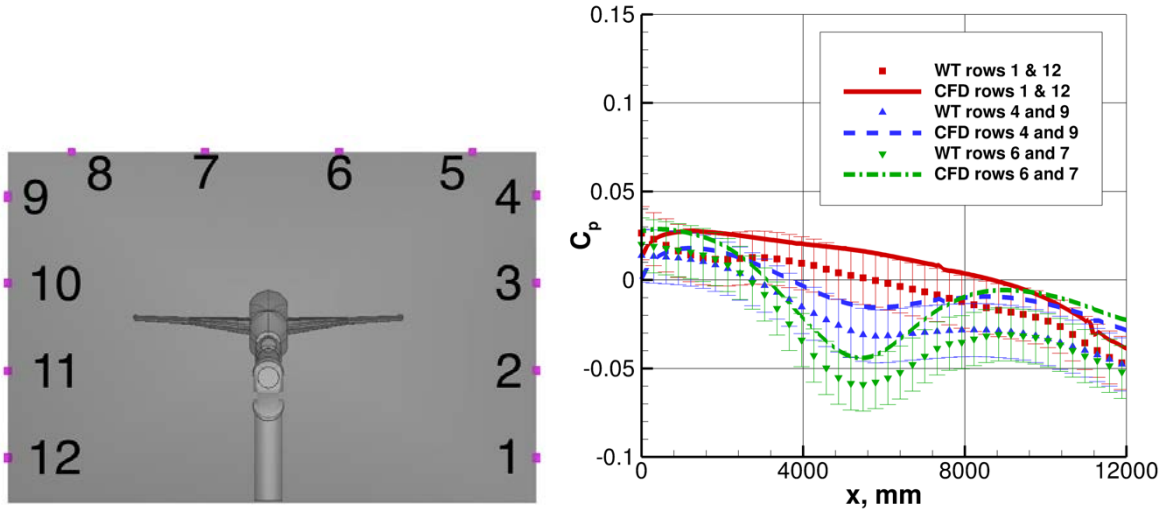

Figure 6: Tunnel wall pressure tap locations (left) and comparisons with CFD wall pressure coefficients (right) at AoA=5º.

In situ laser scans of the JF test article were performed in the 14x22 (wind off). This scanning allowed for direct comparisons with the as-designed test article shape, but alignment can be challenging. Also, compared to the as-designed shape, the measured shape may be somewhat influenced by aeroelastic deflections due to gravity. By allowing CAD software to find the "best fit," the estimated root-mean-square (RMS) deviation of the as-built JF shape compared to the as-designed shape (taken over the entirety of the test article) appeared to be near 0.472 mm for the 2018 scan and 0.597 mm for the 2020 scan. These are both larger than the estimated paint thickness of 0.254-0.356 mm. The reason for the difference is unknown. The reason for the larger RMS deviation in 2020 compared to 2018 is also not known. Both measurements were done in the same way, and with the same claimed measurement accuracy of 0.1 mm. It is not yet clear if any of the scanned differences are significant or not, from a CFD perspective. Nor is it clear precisely how to make use of the scanned information in a CFD analysis. Attempts to use the scanned data to create a usable CAD surface (without extraneous wiggles and steps that are clearly not present in the real model and that yield nonsensical CFD results) have failed to date.

There are two ways that laser scans have proved to be very useful for CFD analysis during the JF effort. The first is as an aid to determine precise positioning of the test article in the wind tunnel at each of the angles of incidence tested. The second is to very accurately assess the locations of the trip dots that were installed by hand on the fuselage and wings.

The aeroelastic deflections of the JF wings have been measured via photogrammetry during wind-on conditions. At an incidence angle of 5 degrees, the wing tip deflected up approximately 2 mm, with a negative twist angle of less than 0.1 degrees. This very small amount of deflection and twist may have some small effect at the most outboard stations, but it is not believed to have any significant influence in the wing root region of interest, compared to a perfectly rigid wing. However, to date, this has not been confirmed by any CFD studies. The test article was supplied with an on-board measurement of the incidence angle (relative to the gravity vector), so, regardless of the aeroelastic deflections of the mast/sting, the model itself was positioned nominally at the prescribed incidence angles relative to the tunnel centerline.

3.0 CFD STUDIES

This section highlights lessons learned from CFD studies of the NASA JF configuration to date. It includes the influence of wind tunnel walls and a summary of where CFD currently stands in its ability to accurately compute juncture flows.

3.1 Influence of Wind Tunnel Walls

Some strategies for running the JF tunnel cases with CFD [11,12,14,26] are summarized here. Refer back to Figure 2 for a picture of the CFD tunnel configuration. Note that CFD has been run both with and without the mast and sting included. Including the tunnel's upstream contraction was found to be important for achieving the best match with inflow boundary conditions, including boundary-layer thickness at the walls and flow angularity in the test section. We opted to treat the tunnel walls as viscous walls. Treating them inviscidly may be a reasonable approximation in some circumstances, but it loses any influence of boundary-layer growth in the test section. Including the diffuser appears to be less important than including the contraction, at least for cases where the test article is not located far downstream in the test section (in the 14x22, the wings of the JF model were located somewhere near x = 6-7 m out of total 15.24 m test section length). Because inclusion of the diffuser often caused problems in the CFD due to separation (forward flow) occurring at the outflow boundary, we devised several different strategies for preventing the CFD from failing: (1) adding a constant-area extension to the downstream exit of the diffuser, as shown in Figure 2 (this "contains" any diffuser separation, keeping it from the outflow boundary of the CFD domain), (2) removing the diffuser altogether, leaving only the contraction and test section, (3) removing the diffuser and extending the test section (making it longer), and (4) employing inviscid walls in the diffuser section only. At this time, we have not seen any clear advantage of one of these methods over another; they each appear to yield reasonable flow in the region of the test section where the model is located. However, methods (2) and (3) do cause the computed tunnel wall pressures to differ significantly from the measured results over the rear half of the test section.

We found it helpful to use the same coordinate system in the tunnel runs as in the free-air runs, with the origin at the test article nose and the x axis along the fuselage centerline. This coordinate system matched the one used in the WT measurements, and allowed for direct and simplified postprocessing (particularly of the Reynolds stress components). The inclusion (or lack thereof) of the mast and sting in the CFD did not have a significant impact

on the JF quantities of interest. However, when including the mast, it typically produced locally unsteady flow that could inhibit convergence when trying to run the CFD to steady state.

The procedure for running the CFD with wind tunnel walls was as follows. Isentropic thermodynamic relations with the desired reference Mach number (M = 0.189) were used to obtain total pressure (p_t/p_{ref}) and total temperature (T_t/T_{ref}) at the tunnel inlet. An appropriate inlet BC that uses these total values was applied at the leftmost boundary in Figure 2; this inlet BC remained unchanged throughout the iterative procedure. In the iterative procedure, a back pressure was set at the rightmost boundary shown in the same figure and a CFD solution obtained. Computed values of total pressure, static pressure, and total temperature at specific probe locations were then used in conjunction with the 14x22 wind tunnel calibration equations to obtain the attained reference conditions (in most cases Reynolds number). Then the back pressure was adjusted iteratively until the desired conditions were reached. This iterative procedure has also been automated [33].

Officially, for establishing the best one-to-one correspondence between the CFD and experimental conditions, we believe that the CFD should run the NASA JF case with the wind tunnel walls included. However, we have discovered some issues with this procedure.

1. Because the CFD has to iterate on its back pressure to obtain the correct flowfield in the test section for each of its in-tunnel runs, consistency is sometimes forfeited. In other words, different CFD codes may perform this iterative procedure differently, yielding different results (even with the same turbulence model).
2. There are subtleties regarding how to establish reference conditions in the wind tunnel. The 14x22 has its own calibration procedure, and to be strictly correct, the CFD needs to mimic this same procedure [33], which still yields some minor inconsistencies. Programming this nontrivial procedure in different CFD codes may also introduce errors or differences.
3. It is more difficult to iteratively converge in-tunnel CFD computations, compared with free-air computations, especially when including the support hardware (sting and mast).

Because of the above problems, when validating CFD methodology effectiveness, turbulence model effectiveness, or to explore new modeling ideas, the use of free-air computations has been preferable to date. We have expended considerable effort to establish the impact and importance of wind tunnel walls on the NASA JF quantities of interest [10,11,14], in order to ascertain whether free-air computations are reasonable approximations in this case. (Note: the free-air runs do not make use of any angle-of-attack corrections.)

Because the JF test article was full span and centrally-placed in the tunnel, we have found that the influence of the wind tunnel walls primarily manifests itself in a slightly more pronounced suction peak near the wing leading edge, compared to free air. Also, the *w* component of edge velocity near the test article is sometimes shifted a very small amount. However, the main quantities of interest for us – the separation bubble size and general flowfield details such as mean flow and Reynolds stress components – are not affected significantly. Clearly, inclusion of the wind tunnel walls would be far more crucial for CFD in the case of a semispan wall-mounted test article. Figure 7 shows flowfield details near the junction corner approaching separation for two CFD codes (FUN3D and OVERFLOW) using the Spalart-Allmaras (SA) turbulence model with Rotation-Curvature (RC) correction and Quadratic Constitutive Relation (QCR) (SA-RC-QCR2013-V) [14,34-36], both with and without wind tunnel walls. Differences between free-air and in-tunnel computations are visible (comparable to differences caused by discretization error), but are generally small relative to the differences between CFD and experiment. Our studies [11,14,26] also indicate minimal impact of tunnel walls on separation size. Based on these studies,

we are convinced that the character of the JF flow is represented well enough by free-air computations so as to still be useful for quantitative evaluation of CFD in the corner region.

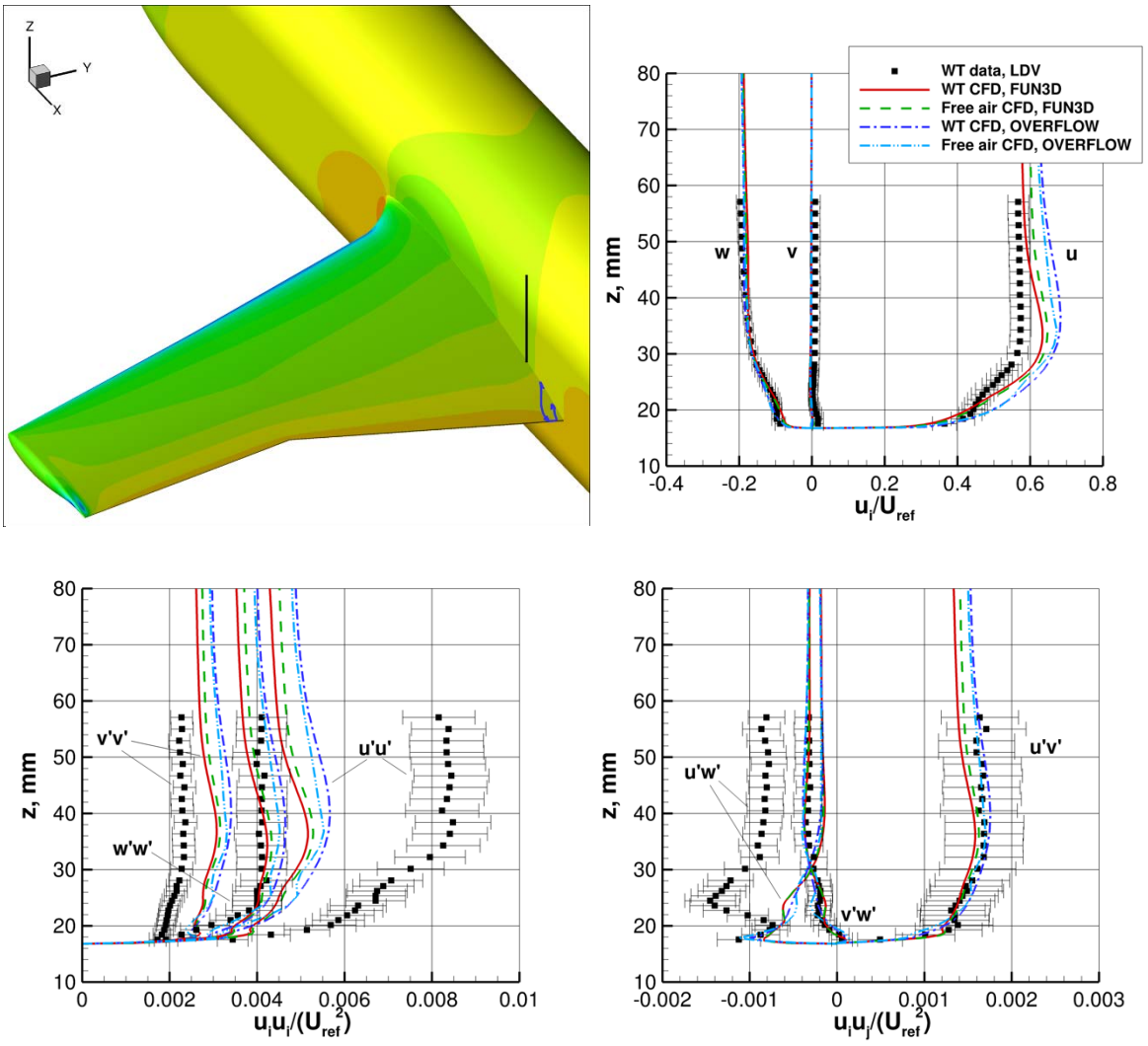

Figure 7: Velocity and turbulent Reynolds stresses near the corner for NASA JF at AoA=5º, SA-RC-QCR2013-V turbulence model, x=2747.6 mm, y=-237.1 mm (profiles are taken along the black line in top left figure).

3.2 Summary of CFD's Capability to Accurately Predict Juncture Flow

Throughout the JF CFD validation experiment, we have made conclusions regarding the capability of particular Reynolds-averaged Navier-Stokes (RANS) turbulence models to predict this flow. Many of these conclusions have been bolstered by the fact that two independent CFD codes have been employed by the team throughout, and both codes have undergone extensive code verification efforts [8] in an attempt to guarantee correct and consistent code implementation of the turbulence models being evaluated [9,14]. Efforts have also been made to assess the

impact of numerical discretization error [10,14]. Although details of the grid convergence studies are not shown here, the general conclusions are as follows. For RANS, using state-of-the-art grids with $\mathcal{O}(10^8)$ degrees of freedom and appropriate grid spacings, numerical error has been found to be acceptably low over most of the test article, but it tended to be significantly higher in and near separation. For the interested reader, the plotted comparisons in Rumsey et al. [10] included CFD error bars, which can be unrealistically large near separation because even small movement of the predicted separation location causes very large changes to the flowfield at any given point in space. The general conclusions for JF have been consistent with other independent studies (e.g., Ref. [37]). For example, we have confirmed that linear eddy viscosity models (which make use of the Boussinesq constitutive relation) tend to predict JF corner separation far too early, with the separation region too long by as much as 100% or more. The use of nonlinear constitutive relations such as QCR2013-V have yielded dramatically improved results.

For corner flows like JF, we believe a key measure of success for CFD is its ability to accurately predict stress-induced vortices that evolve along corners in turbulent flow [9,14]. These structures are driven and maintained by differences in the flowfield's Reynolds normal stresses (particularly $\langle v'v' \rangle$ and $\langle w'w' \rangle$ for flow along a corner that is mostly aligned with the x direction) [38]. For RANS, nonlinear modeling is typically required for any hope of predicting normal stresses reasonably accurately. (Note that accurate prediction of normal stresses is generally not considered important in CFD for attached flows well away from corners.) In our particular JF configuration, we have seen evidence of one stress-induced vortex residing within a few mm of the wing-fuselage junction in both the LDV measurements and in the CFD. Figure 8 shows this vortex from a CFD computation. We believe that this particular stress-induced vortex plays a pivotal role in delaying the onset of separation in the JF corner. Thus, if a turbulence model fails to capture Reynolds normal stress differences reasonably well, it fails to correctly predict the stress-induced vorticity in the corner, and separation onset is consequently mispredicted.

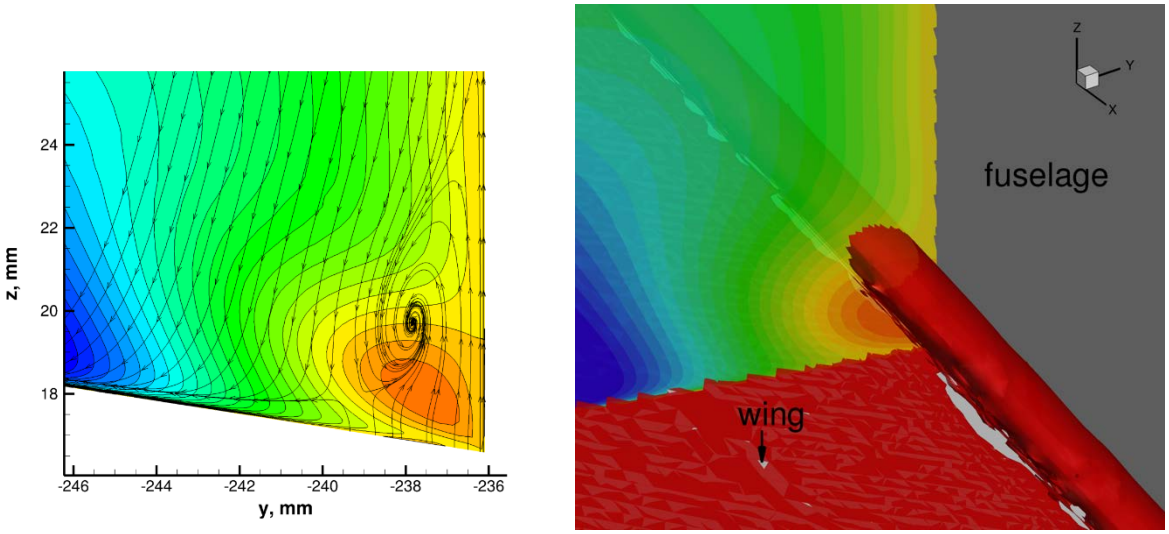

Figure 8: Contours of v-velocity with in-plane modified streamlines (left) and isocontour of Q criterion (right) showing stress-induced vortex near JF corner at x=2747.6 plane upstream of separation, SA-RC-QCR2013-V model.

With the very high quality of the NASA JF wind tunnel LDV data, along with its uncertainty estimates [7-9, 39], we have been able to discern cause-and-effect relationships and patterns between Reynolds stress predictions and separated flow predictions. In fact, although the SA-RC-QCR2013-V nonlinear model dramatically improves predictions compared with the SA-RC linear model, it still predicts separation onset somewhat too early (with separation size predicted roughly 30% too long). With the insights and intuition garnered from comparisons between CFD and LDV, a new version of QCR was devised [40]. This model, termed QCR2020, predicts JF separation with very little error over a range of angles of incidence. Furthermore, the model was found to improve predicted corner flow results in an independent case.

An example showing the improvement in prediction of normal stresses for JF using the new version of QCR is shown in Figure 9. In particular, near the wall, the separation (or difference) between $\langle v'v' \rangle$ and $\langle w'w' \rangle$ is improved with QCR2020 compared with QCR2013-V. Also, QCR2020 produces a larger near-wall peak value in $\langle u'u' \rangle$, although it is still low compared with WT data. Wing surface separation patterns are shown in Figure 10. SA-RC-QCR2013-V predicts separation somewhat too early at all angles of incidence, whereas SA-RC-QCR2020 is more accurate compared with locations determined from oil flow. The development of QCR2020, arising directly from the NASA JF effort, is a testament to the value of CFD validation experiments, particularly when validation dialog and technique verification play a central role [41].

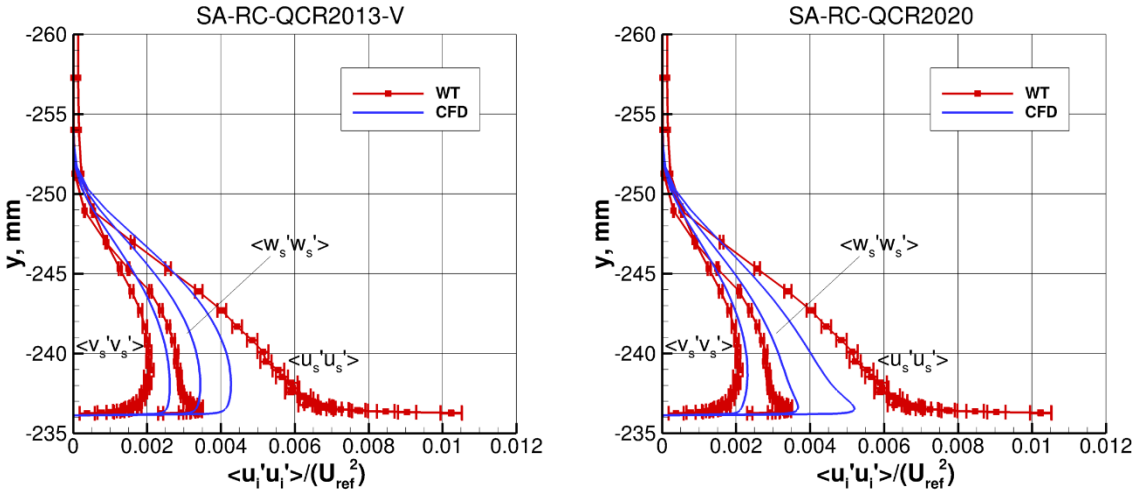

Figure 9: Reynolds normal stress predictions on side of fuselage nose, x=1168.4 mm, z=0 mm, AoA=5°.

It is important to note that although the SA-RC-QCR2020 model significantly improves predictions of where separation occurs (including the flow leading up to separation [9]), it is still deficient post separation, i.e., within the separated region itself. This behavior is consistent with many other RANS studies of separated flow, which seem to suggest that RANS may be fundamentally deficient in predicting the underlying physics inside of an unsteady turbulent separation region. Also, as mentioned earlier, it appears to be very difficult for RANS to obtain highly grid-converged results in and near the JF separated region; it is recommended that future work focuses on the use of grid adaption in an effort to resolve this issue.

All RANS models investigated to date (including SA-RC-QCR2020) have particular difficulty predicting the $\langle u'u' \rangle$ component of the Reynolds normal stresses very near walls. As discussed in Ref. [9], this component is

not as important as $\langle v'v' \rangle$ and $\langle w'w' \rangle$ for capturing the mean flow. Nonetheless, errors in this streamwise normal stress component can negatively impact other Reynolds stress components when the flow is not aligned perfectly with the x axis. Therefore, care needs to be exercised when drawing conclusions from comparisons of the various Reynolds stress components.

Most RANS turbulence model evaluations to date have been done with the models run fully turbulent. We learned that forcing transition to occur on the fuselage at the nose trip dots (near x = 336 mm) reduces the predicted fuselage boundary-layer thickness downstream by a few mm compared to a fully turbulent calculation. This change yields better agreement with measured boundary-layer thickness; however, it has been found to have little influence on the separation size/extent or essential flowfield details in the corner region. There has been less experience with the influence of forcing transition on the wings, although Eisfeld et al. [16] experimented using CFD and found relatively small influence on JF quantities of interest.

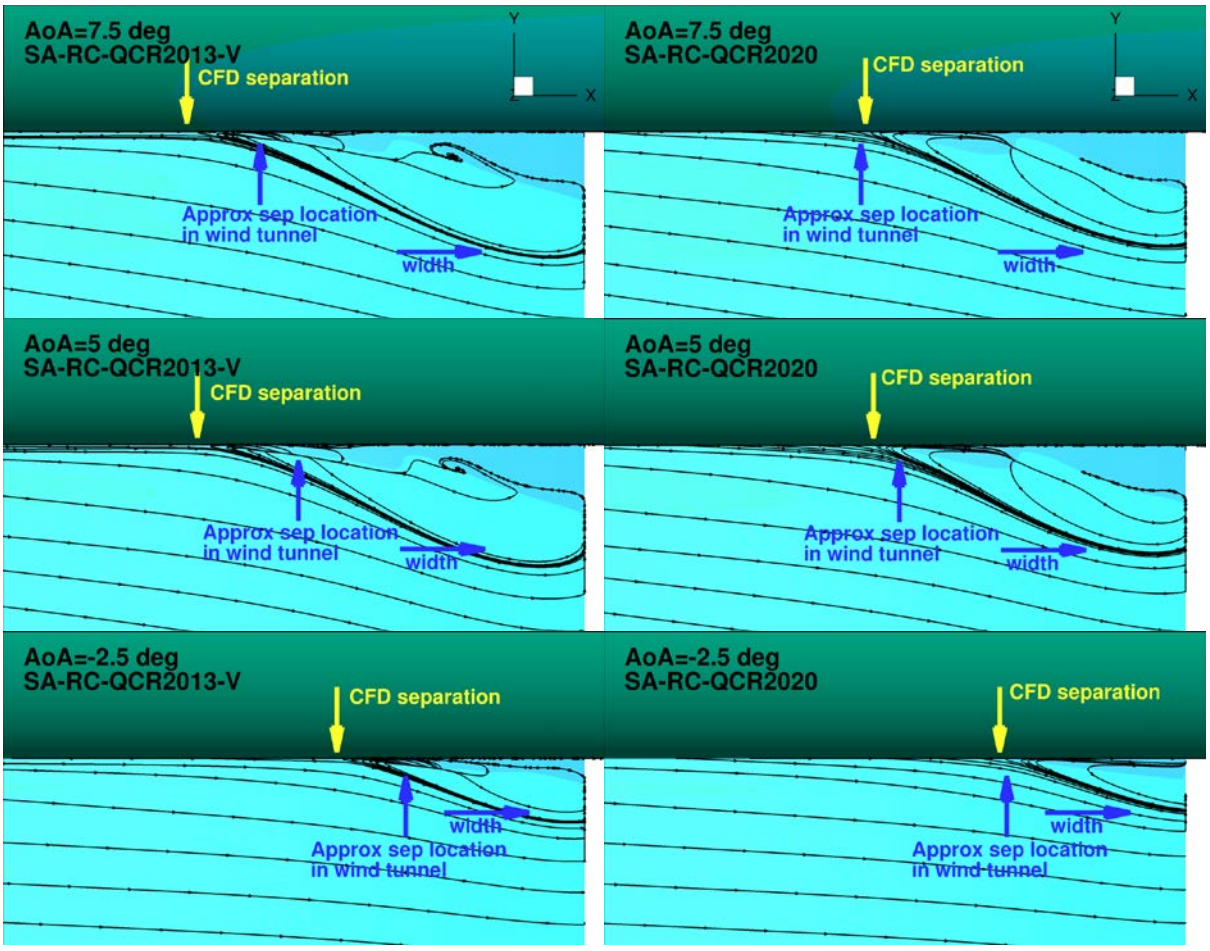

Figure 10: Surface streamlines from CFD show computed separation regions; blue arrows indicate oil flow separation size from the wind tunnel test; using QCR2013-V (left) and QCR2020 (right).

As mentioned in the Introduction, in addition to the JF team's work, other independent CFD efforts have been conducted, mostly as part of AIAA special sessions. Here, we provide a brief synopsis of what we have learned from this other work to date. The reader is referred to the original AIAA papers [14-29] for additional details. Among RANS models, a 7-equation second-moment Reynolds-stress transport (RST) model [16] appeared to

predict corner separation size well, although it was still deficient in the prediction of some flowfield details. However, different RST models [22, 23] produced inconsistent results, which in one case was very poor. With a few exceptions, most other RANS turbulence models appeared to predict similar JF results to each other, with separation typically predicted too early. All RANS models (even RST) had particular difficulty predicting the $\langle u'u' \rangle$ component of the Reynolds normal stresses very near walls. Also, near the corner all RANS models tended to predict an excess of streamwise momentum (see, e.g., the u component of velocity in Figure 7(b) above), for unknown reasons. In some cases, different RANS codes with ostensibly the same turbulence model yielded inconsistent results, suggesting possible issues with verification in some codes.

A variety of scale-resolving methods have been applied to the JF case, including wall-modeled large eddy simulation (WMLES), hybrid RANS-LES, and Lattice Boltzmann. Generally, these methods tend to have the opposite problem of RANS, in that they predict separation too late (or not at all). At this time, the reason for this tendency is not known. All of these methodologies are considerably more expensive than RANS, so it can be difficult to demonstrate grid-converged results. In the particular case of hybrid RANS-LES, sometimes grid refinement has led to poorer results, because of issues related to failure of the shielding function (which may incorrectly push the interface between the RANS and LES regions into the boundary layer). Boundary-layer tripping, which is required for LES, wall-modeled LES, and Lattice-Boltzmann, can be difficult and costly, but new strategies are being tested and advanced as work in these areas progress.

4.0 SUMMARY AND FUTURE DIRECTIONS

The NASA JF effort has yielded a wealth of data to date, as well as a modification to a widely used turbulence constitutive relation that has led to improved predictions both for JF and other independent cases. In addition, lessons have been gleaned from both the wind tunnel measurements and the concomitant CFD analysis, both essential components of the CFD validation experiment. This paper has presented many of these insights.

In any CFD validation experiment, it is crucial that CFD and wind tunnel measurements are "comparing apples with apples," in the sense that all boundary conditions and geometric details are as identical as possible. Therefore, expending a significant effort on wind tunnel characterization (including test article characterization) is a necessary component of a well-run CFD validation experiment. Unfortunately, wind tunnel characterization is not always easy or possible, especially at the tunnel inflow of many existing facilities with little or no optical access. Furthermore, it is not always easy in CFD to make use of nontraditional boundary-condition information, because such computational capability is not typically available. Even laser-based characterization of the test article shape is not readily translatable to a usable CFD configuration/grid with today's state-of-the-art tools. This paper has summarized the efforts made in wind tunnel characterization during the JF CFD validation experiment, and has discussed some of their implications.

Although running CFD with wind tunnel walls is generally the best way to try to closely match wind tunnel measurement conditions, there can be CFD-related problems that accompany it. These include difficulties with consistency and convergence. Some strategies for running CFD with wind tunnel walls and overcoming such problems were discussed. It was also shown that CFD can be used to help quantify the influence of the wind tunnel on quantities of interest. If the influence is small enough, then free-air computations can be used quite successfully in conjunction with the wind tunnel data to validate models and provide information and inspiration to guide model improvements.

The current status of CFD's state-of-the-art ability to accurately predict juncture flow separation was summarized. A key aspect seems to be the need for CFD to reasonably capture Reynolds normal stresses in the corner region,

which leads to stress-induced streamwise vortex/vortices that act to delay the onset of separation. Most existing RANS CFD turbulence models tend to predict separation too early, with linear eddy viscosity turbulence models generally the worst because they cannot predict stress-induced vorticity at all. Second-moment Reynolds stress transport models appear to be able to predict the JF separation well, but some details are missed and different model versions yield very different results. Scale-resolving simulations to date have typically yielded the opposite problem to most of the traditional RANS methods: they tend to predict separation somewhat too late or not at all. However, many of these simulation methodologies are still emerging, and may require time to evolve their capabilities.

The two CFD codes used in the NASA JF effort were verified for the particular turbulence models used (and they yielded consistent solutions). However, a lack of consistency seems to still be a problem among some CFD codes that ostensibly have the same turbulence models implemented. This lack of code verification makes it more difficult to draw conclusions regarding model capability.

One of the strengths of the NASA JF team was its effective validation dialog between its CFD and measurement specialists. However, even greater integration and collaboration is always possible. For example, cross-training individuals to some extent may be useful, leading to better understanding of the capabilities and limitations of each discipline. Regular and persistent communication is important because it helps to break down barriers. The next phase of the NASA JF experiment is to test a different wing shape (with NACA 0015 profile at the root), which is designed to achieve a range of results from no corner separation to small/incipient separation. This additional validation case will further challenge the CFD models. It should either lead to greater confidence in those models that already work reasonably well, or else provide additional information that may lead to further improvements in the models.

ACKNOWLEDGMENTS

The author thanks all of the members of the NASA JF team, past and present, who have helped to make this such a successful project. This work was supported by the NASA Transformational Tools and Technologies (TTT) project of the Transformative Aeronautics Concepts Program.

REFERENCES

[1] Rumsey, C. L., Neuhart, D. H., and Kegerise, M. A., "The NASA Juncture Flow Experiment: Goals, Progress, and Preliminary Testing," AIAA-2016-1557, January 2016, doi: https://doi.org/10.2514/6.2016-1557.

[2] Vassberg, J. C., Tinoco, E. N., Mani, M., Brodersen, O. P., Eisfeld, B., Wahls, R. A., Morrison, J. H., Zickuhr, T., Laflin, K. R., Mavriplis, D. J., "Abridged Summary of the Third AIAA Computational Fluid Dynamics Drag Prediction Workshop," *AIAA Journal of Aircraft*, Vol. 45, No. 3, May–June 2008, pp. 781–798, doi: https://doi.org/10.2514/1.30572.

[3] AIAA-G-077-1998(2002), "Guide for the Verification and Validation of Computational Fluid Dynamics Simulations," January 1998, re-affirmed June 2002, doi: https://arc.aiaa.org/doi/abs/10.2514/4.472855.

[4] Lee, H. B., Ghia, U., Bayyuk, S., Oberkampf, W. L., Roy, C. J., Benek, J. A., Rumsey, C. L., Powers, J. M., Bush, R. H., and Mani, M., "Development and Use of Engineering Standards for Computational Fluid Dynamics for Complex Aerospace Systems," AIAA-2016-3811, June 2016, doi: https://doi.org/10.2514/6.2016-3811.

[5] Oberkampf, W. L. and Smith, B. L., "Assessment Criteria for Computational Fluid Dynamics Model Validation Experiments," *Journal of Verification, Validation and Uncertainty Quantification*, Vol. 2, No. 3, 031002, September 2017, pp. 1-14, doi: https://doi.org/10.1115/1.4037887.

[6] Taylor, N. J. and Rumsey, C. L., "CFD Validation Experiments: Toward a Broader Perspective," AIAA-2021-1933, January 2021, doi: https://doi.org/10.2514/6.2021-1933.

[7] Kegerise, M. A. and Neuhart, D. H., "An Experimental Investigation of a Wing-Fuselage Junction Model in the NASA Langley 14- by 22-Foot Subsonic Tunnel," NASA/TM-2019-220286, June 2019, https://ntrs.nasa.gov/citations/20190027403.

[8] Rumsey, C. L., "NASA Langley Turbulence Modeling Resource Website," https://turbmodels.larc.nasa.gov, Accessed: 2021-01-25.

[9] Rumsey, C. L., Ahmad, N. N., Carlson, J.-R., Kegerise, M. A., Neuhart, D. H., Hannon, J. A., Jenkins, L. N., Yao, C.-S., Balakumar, P., Gildersleeve, S., Bartram, S. M., Pulliam, T. H., Olsen, M. E., and Spalart, P. R., "CFD Comparisons with Updated NASA Juncture Flow Data," AIAA-2021-1427, January 2021, doi: https://doi.org/10.2514/6.2021-1427.

[10] Rumsey, C. L., Carlson, J.-R., Ahmad, N. N., "FUN3D Juncture Flow Computations Compared with Experimental Data," AIAA-2019-0079, January 2019, doi: https://doi.org/10.2514/6.2019-0079.

[11] Lee, H. C., Pulliam, T. H., "Overflow Juncture Flow Computations Compared with Experimental Data," AIAA-2019-0080, January 2019, doi: https://doi.org/10.2514/6.2019-0080.

[12] Rumsey, C. L., Carlson, J.-R., Hannon, J. A., Jenkins, L. N., Bartram, S. M., Pulliam, T. H., Lee, H. C., "Boundary Condition Study for the Juncture Flow Experiment in the NASA Langley 14x22-Foot Subsonic Wind Tunnel," AIAA-2017-4126, June 2017, doi: https://doi.org/10.2514/6.2017-4126.

[13] Lee, H. C., Pulliam, T. H., Neuhart, D. H., and Kegerise, M. A., "CFD Analysis in Advance of the NASA Juncture Flow Experiment," AIAA-2017-4127, June 2017, doi: https://doi.org/10.2514/6.2017-4127.

[14] Rumsey, C. L., Lee, H. C., Pulliam, T. H., "Reynolds-Averaged Navier-Stokes Computations of the NASA Juncture Flow Model Using FUN3D and OVERFLOW," AIAA 2020-1304, January 2020, doi: https://doi.org/10.2514/6.2020-1304.

[15] Abdol-Hamid, K. S., Ahmad, N. N., Carlson, J.-R., Biedron, R. T., "Juncture Flow Computations using kL-Based Turbulence Models," AIAA 2020-1305, January 2020, doi: https://doi.org/10.2514/6.2020-1305.

[16] Eisfeld, B., Togiti, V., Braun, S., Stürmer, A., "Reynolds-Stress Model Computations of the NASA Juncture Flow Experiment," AIAA 2020-1306, January 2020, doi: https://doi.org/10.2514/6.2020-1306.

[17] Iyer, P. S., Malik, M. R., "Wall-Modeled LES of the NASA Juncture Flow Experiment," AIAA 2020-1307, January 2020, doi: https://doi.org/10.2514/6.2020-1307.

[18] Lozano-Duran, A., Moin, P., Bose, S. T., "Prediction of Trailing Edge Separation on the NASA Juncture Flow Using Wall-Modeled LES," AIAA 2020-1776, January 2020, doi: https://doi.org/10.2514/6.2020-1776.

[19] Balin, R., Wright, J. R., Patterson, J. W., Farnsworth, J., Evans, J., Lakhani, R., Spalart, P. R., Jansen, K. E., "Hybrid Turbulence Model Computations of the NASA Juncture Flow Model Using PHASTA," AIAA 2020-1777, January 2020, doi: https://doi.org/10.2514/6.2020-1777.

[20] Duda, B., Laskowski, G. M., "Lattice Boltzmann Very Large Eddy Simulations of the NASA Juncture Flow Model," AIAA 2020-1778, January 2020, doi: https://doi.org/10.2514/6.2020-1778.

[21] Ghate, A. S., Housman, J. A., Stich, G.-D., Kenway, G. K., and Kiris, C. C., "Scale Resolving Simulations of the NASA Juncture Flow Model Using the LAVA Solver," AIAA Paper 2020-2735, June 2020, doi: https://doi.org/10.2514/6.2020-2735.

[22] Zastawny, M. and Lardeau, S., "Application of Simcenter STAR-CCM+ for Assessment of the Impact of CFD Modelling Approach in NASA Juncture Flow Simulations," AIAA Paper 2020-2736, June 2020, doi: https://doi.org/10.2514/6.2020-2736.

[23] Aliaga, C. N., Chen, J., Selvanayagam, J., Ozcer, I. A., and Stokes, J., "Automatic Mesh Optimization for Wing-Fuselage Juncture Flow Separation Predictions," AIAA Paper 2020-2750, June 2020, doi: https://doi.org/10.2514/6.2020-2750.

[24] Wood, S. L., Anderson, W. K., Park, M. A., Balan, A., Karman, S., and Jacobson, K. E., "Reynolds-Averaged Navier-Stokes Computations of the NASA Juncture Flow Model Using Expert-Crafted and Adapted Grids," AIAA Paper 2020-2751, June 2020, doi: https://doi.org/10.2514/6.2020-2751.

[25] Abe, H., Mizobuchi, Y., and Matsuo, Y., "Effect of a Quadratic Constitutive Relation on Juncture Flow Computations," AIAA Paper 2020-2752, June 2020, doi: https://doi.org/10.2514/6.2020-2752.

[26] Ahmad, N. N., Rumsey, C. L., and Carlson, J.-R., "In-Tunnel Simulations of the NASA Juncture Flow Model," AIAA-2021-1428, January 2021, doi: https://doi.org/10.2514/6.2021-1428.

[27] Olsen, M. E., "Lag Model Prediction of the NASA Juncture Flow," AIAA-2021-1429, January 2021, doi: https://doi.org/10.2514/6.2021-1429.

[28] Duda, B. and Laskowski, G., "Simulating the NASA Juncture Flow Model with a Scale-Resolving Lattice-Boltzmann Method, AIAA-2021-1743, doi: https://doi.org/10.2514/6.2021-1743.

[29] Diskin, B., Ahmad, N., Anderson, W. K., Derlaga, J. M., Pandya, M. J., Rumsey, C. L., Wang, L., Wood, S. L., Liu, Y., Nishikawa, H., and Galbraith, M. C., "Verification Test Suite for Spalart-Allmaras QCR2000 Turbulence Model, AIAA-2021-1552, doi: https://doi.org/10.2514/6.2021-1552.

[30] Kusunose, K. and Crowder, J., "Extension of Wake-Survey Analysis Method to Cover Compressible Flows," AIAA Journal of Aircraft, Vol. 39, No. 6, 2002, pp. 954–963, doi: https://doi.org/10.2514/2.3048.

[31] Masseboeuf, S., Mouton, S., Mariani, R., and Leclaire, B., "Clinometric Measurements by Means of High-Accuracy PIV in the ONERA F1 Low Speed Pressurized Wind Tunnel," 13th Asian Symposium on Visualization, Novosibirsk, Russia, June 2015.

[32] Nayani, S. N., Sellers, W., Brynildsen, S. E., and Everhart, J. L., "Numerical Study of the High-Speed Leg of a Wind Tunnel," AIAA-2015-2022, January 2015, doi: https://doi.org/10.2514/6.2015-2022.

[33] Carlson, J., "Automated Boundary Conditions for Wind Tunnel Simulations," NASA/TM-2018-219812, March 2018, https://ntrs.nasa.gov/citations/20180002095.

[34] Spalart, P. R., Allmaras, S. R., "A One-Equation Turbulence Model for Aerodynamic Flows," *Recherche Aerospatiale*, Vol. 1, 1994, pp. 5–21.

[35] Shur, M. L., Strelets, M. K., Travin, A. K., and Spalart, P. R., "Turbulence Modeling in Rotating and Curved Channels: Assessing the Spalart-Shur Correction," *AIAA Journal*, Vol. 38, No. 5, 2000, pp. 784–792, doi: https://doi.org/10.2514/2.1058.

[36] Spalart, P. R., "Strategies for Turbulence Modelling and Simulations," *International Journal of Heat and Fluid Flow*, Vol. 21, 2000, pp. 252–263.

[37] Bordji, M., Gand, F., Deck, S., and Brunet, V., "Investigation of a Nonlinear Reynolds-Averaged Navier-Stokes Closure for Corner Flows," *AIAA Journal*, Vol. 54, No. 2, 2016, pp. 386–398, doi: https://doi.org/10.2514/1.J054313.

[38] Perkins, H. J., "The Formation of Streamwise Vorticity in Turbulent Flow," Journal of Fluid Mechanics, Vol. 44, Part 4, 1970, pp. 721–740, doi: https://doi.org/10.1017/S0022112070002112.

[39] Aeschliman, D. P. and Oberkampf, W. L., "Experimental Methodology for Computational Fluid Dynamics Code Validation," *AIAA Journal*, Vol. 36, No. 5, 1998, pp. 733–741, doi: https://doi.org/10.2514/2.461.

[40] Rumsey, C. L., Carlson, J.-R., Pulliam, T. H., and Spalart, P. R., Improvements to the Quadratic Constitutive Relation Based on NASA Juncture Flow Data," *AIAA Journal*, Vol. 58, No. 10, 2020, pp. 4374-4384, doi: https://doi.org/10.2514/1.J059683.

[41] Rumsey, C. L., "The NASA Juncture Flow Test as a Model for Effective CFD/Experimental Collaboration," AIAA Paper 2018-3319, June 2018, doi: https://doi.org/10.2514/6.2018-3319.